

Negative dynamic conductivity of the photoinduced η pairing state

Satoshi Ejima^{1,2} and Benedikt Fauseweh^{3,4}

¹ *Institute of Software Technology, German Aerospace Center (DLR), 22529 Hamburg, Germany*

² *Computational Condensed Matter Physics Laboratory,*

RIKEN Cluster for Pioneering Research (CPR), Saitama 351-0198, Japan

³ *Institute of Software Technology, German Aerospace Center (DLR), 51147 Cologne, Germany*

⁴ *Department of Physics, TU Dortmund University, Otto-Hahn-Str. 4, 44227 Dortmund, Germany*

(Dated: September 10, 2024)

We report the observation of a sharp dynamic negative optical conductivity, $\sigma(\omega; t)$, above the equilibrium Mott gap $\omega > \Delta_c$, after an electromagnetic pump pulse in the half-filled Hubbard chain. The negative peak in the real part of $\sigma(\omega; t)$ is a distinctive hallmark of the photoinduced η -pairing state, distinguishing it from phases dominated by incoherent doublon formation, which do not exhibit this feature. The negative conductivity and its dynamic oscillations, observed in the absence of continuous driving, are indicative of a nonequilibrium excitation, akin to the Higgs mode observed in s- and d-wave superconductors. We use the time-dependent tensor-network algorithm in the infinite matrix-product-state representation, providing a detailed characterization of the optical response in this nonequilibrium state.

Recent developments in laser technology have revolutionized various scientific fields, enabling exceptional precision and control. Innovations such as ultrafast pulse lasers have opened new frontiers in quantum physics and material science, and have also found significant applications in condensed matter physics, particularly in the study of strongly correlated electron systems [1–3]. Examples include the ultrafast switching of Weyl semimetals [4], anomalous Hall effect in graphene [5] and charge-density waves in rare-earth tritelluride LaTe_3 [6].

A particular interesting prospect is the use of laser pulse femtosecond drives to dynamically induce novel states in quantum materials [7], with light-induced superconductivity as a most prominent example [8–11]. Significant theoretical efforts have been devoted to understanding the conditions under which such exotic nonequilibrium states emerge [12–16], yet the mechanisms and detection of these phases remain under debate.

In this context, one intriguing phenomenon that has attracted attention is the η pairing, first proposed by C. N. Yang for the Hubbard model [17], which represents a state with off-diagonal long-range order that is crucial for understanding high-temperature superconductivity and other quantum phenomena. However, η pairs are absent in the ground state and have received only specific attention, especially from a theoretical point of view. A recent study has shown that pulse irradiation can induce η pairing in the Hubbard model, even in its Mott insulating phase [18]. The nonlinear optical response is crucial in enhancing the number of η pairs, thereby promoting superconducting correlations in the photoexcited state. These findings highlight the potential of nonequilibrium dynamics as a way to access exotic quantum states and enhance superconductivity [19]. The synergy between advanced laser technologies and the Hubbard model provides a promising avenue for exploring new quantum phases and understanding the mecha-

nisms underlying high-temperature superconductivity.

The detection of η pairs in experimental settings presents significant challenges due to the intricate nature of these quantum states. First, the Hamiltonian of the system must preserve the number of η pairs, corresponding to a hidden $\text{SU}(2)$ symmetry. This requirement is not easily met in typical experimental setups, making it difficult to create and maintain the required conditions for η pairs. In addition, the transient nature of photoinduced η pairs adds another layer of complexity. These pairs are typically short-lived and require ultrafast measurement techniques to capture their dynamics. The use of advanced laser systems, such as ultrashort pulse lasers, is essential to induce and probe these states, but even with these tools, the signal can be weak and easily obscured by noise.

As a candidate physical quantity, Kaneko *et al.* demonstrated one of the hallmarks of superconductivity, the nonvanishing charge stiffness of the photoinduced η -pairing states, by analyzing the system-size dependence using the exact diagonalization method [20]. Time- and angle-resolved photoemission spectroscopy experiments would provide us with the signature of the photoinduced insulator-to-metal quantum phase transition [21], while it is still challenging to carry out such an experiment in optical lattices, they are strong candidates to prepare Hubbard-type models. The other candidate might be the entanglement entropy, showing the entanglement growth due to the photoinduced η -pairing state [22], since the von Neumann entropy and the second-order Rényi entropy can be detected in optical lattices [23, 24].

Here, we demonstrate that the nonequilibrium optical conductivity $\sigma(\omega; t)$ shows a characteristic negative spectral weight only for the optimal pump-pulse parameter set, which maximally enhances photoinduced η -pairing state. The integrated negative spectral weights $f(t)$ coincide almost perfectly with those from the pair corre-

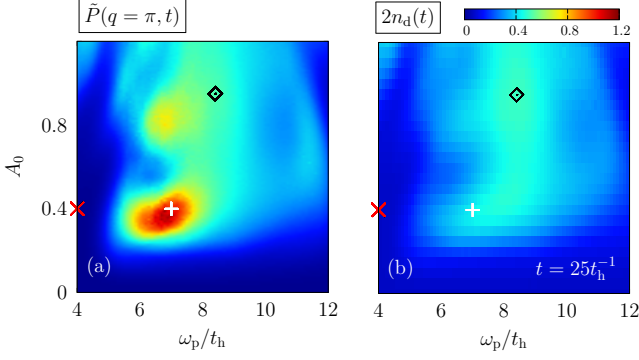


FIG. 1. Contour plots of $\tilde{P}(q = \pi, t)$ (a) and $2n_d(t)$ at $t = 25t_h^{-1}$ in the ω_p - A_0 plane for the half-filled Hubbard chain with $U/t_h = 8$, obtained by iTEBD.

lations after the Fourier transformation. The time dependence of $f(t)$ shows coherent oscillations similar to previously reported Higgs oscillations in conventional s-wave and unconventional d-wave superconductors [25].

The Hamiltonian of the one-dimensional (1D) half-filled Hubbard model is defined as

$$\hat{H} = -t_h \sum_{j,\sigma} (\hat{c}_{j,\sigma}^\dagger \hat{c}_{j+1,\sigma} + \text{H.c.}) + U \sum_j (\hat{n}_{j,\uparrow} - 1/2)(\hat{n}_{j,\downarrow} - 1/2), \quad (1)$$

where $\hat{c}_{j,\sigma}^\dagger$ ($\hat{c}_{j,\sigma}$) is the creation (annihilation) operator of an electron with spin projection $\sigma \in \{\uparrow, \downarrow\}$ at lattice site j , and $\hat{n}_{j,\sigma} = \hat{c}_{j,\sigma}^\dagger \hat{c}_{j,\sigma}$ is the number operator. t_h and U are nearest-neighbor hopping amplitude and on-site Coulomb repulsion ($U > 0$), respectively. The so-called η operators, introduced in the seminal paper by Yang [17], construct exact eigenstates of the Hubbard model,

$$\hat{\eta}^+ = \sum_j (-1)^j \hat{\Delta}_j^\dagger \equiv \sum_j \hat{\eta}_j^+, \quad \hat{\eta}^- = (\hat{\eta}^+)^\dagger, \quad (2)$$

$$\hat{\eta}^z = \frac{1}{2} \sum_j (\hat{n}_{j,\uparrow} + \hat{n}_{j,\downarrow} - 1) \equiv \sum_j \hat{\eta}_j^z, \quad (3)$$

which obey the SU(2) commutation relations. Here, $\hat{\Delta}_j^\dagger = \hat{c}_{j,\downarrow}^\dagger \hat{c}_{j,\uparrow}^\dagger$ is the on-site singlet-pair creation operator. Since the Hubbard Hamiltonian (1) commutes with the operator $\hat{\eta}^2 = \frac{1}{2}(\hat{\eta}^+ \hat{\eta}^- + \hat{\eta}^- \hat{\eta}^+) + (\hat{\eta}^z)^2$, so that Hubbard eigenstates are also eigenstates of η^2 , and most importantly eigenstates with a finite value of $\langle \hat{\eta}^2 \rangle$ have long-ranged pairing correlations $\langle \hat{\eta}_j^+ \hat{\eta}_\ell^- \rangle$ [17].

As demonstrated in Ref. [18], η pairs can be induced by applying a pump pulse to Mott insulators described theoretically with the gauge transformation $t_h \hat{c}_{j,\sigma}^\dagger \hat{c}_{j+1,\sigma} \rightarrow t_h e^{iA(t)} \hat{c}_{j,\sigma}^\dagger \hat{c}_{j+1,\sigma}$, where $A(t)$ is the vector potential associated with the external electric field of the pump pulse

$$A(t) = A_0 e^{-(t-t_0)^2/(2\sigma_p^2)} \cos[\omega_p(t-t_0)], \quad (4)$$

where A_0 is the amplitude, ω_p is the frequency and σ_p is the width centered at time $t_0 (> 0)$. This so-called Peierls substitution makes the Hamiltonian time-dependent $\hat{H} \rightarrow \hat{H}(t)$. By utilizing the infinite time-evolved block decimation (iTEBD) technique [26] with second-order Suzuki-Trotter decomposition, the initial ground state evolves in time as $|\psi(0)\rangle \rightarrow |\psi(t)\rangle$. In the following, we take t_h (t_h^{-1}) as the unit of energy (time) and set the time step $\delta t = 0.01 t_h^{-1}$. In this study we use the pump pulse with width $\sigma_p = 2t_h^{-1}$ centered at time $t_0 = 10t_h^{-1}$.

To detect the photoinduced η -pairing state we simulate the time evolution of the pair correlations

$$P(r, t) = \frac{1}{L} \sum_j \langle \psi(t) | \hat{\Delta}_{j+r}^\dagger \hat{\Delta}_j + \text{H.c.} | \psi(t) \rangle \quad (5)$$

and its Fourier transform $\tilde{P}(q, t) = \sum_r e^{iqr} P(r, t)$, where L is the number of lattice sites. Note that the pair correlation at $r = 0$ is equal to the number of double occupancy, $P(0, t) = 2n_d(t) = (2/L) \sum_j \langle \psi(t) | \hat{n}_{j,\uparrow} \hat{n}_{j,\downarrow} | \psi(t) \rangle$.

Figures 1(a) and (b) demonstrate the ω_p and A_0 dependence of $\tilde{P}(q = \pi, t)$ and $2n_d(t)$, respectively, for the time $t = 25t_h^{-1}$, which is related to the nonequilibrium optical conductivity results discussed later. Instead of an artificial stripe structure seen in the previous studies with small clusters [18, 27], the single peak structure appears around $\omega_p/t_h = 7.0$ and $A_0 = 0.4$ in Fig. 1(a) by simulating the system directly in thermodynamic limit ($L \rightarrow \infty$) using iTEBD, while the double occupancy is only slightly enhanced around $\omega_p/t_h \approx U$ as seen in Fig. 1(b). The longer-range contributions of the η -pairing correlations play a significant role around the peak region of Fig. 1(a).

Let us now explain the numerical approach to compute the nonequilibrium optical conductivity. In the presence of $A(t)$ the current operator \hat{J} becomes also time-dependent:

$$\hat{J}(t) = -\frac{\partial \hat{H}(t)}{\partial A(t)} = t_h \sum_{j,\sigma} \left(i e^{iA(t)} \hat{c}_{j,\sigma}^\dagger \hat{c}_{j+1,\sigma} + \text{H.c.} \right). \quad (6)$$

In addition to the pump pulse we apply a weak and narrow probe pulse $A_{\text{pr}}(t) = A_0^{\text{pr}} e^{-(t-t_0^{\text{pr}})^2/2\sigma_{\text{pr}}^2}$, which induces a current deviation $J_{\text{pr}}(t) = \langle \hat{J}_{A+A_{\text{pr}}} \rangle_t - \langle \hat{J}_A \rangle_t$. Setting the probe parameters as $A_0^{\text{pr}} = 0.05$ and $\sigma_{\text{pr}} = 0.05$ with the delay time between pump and probe pulses $\tau = t_0^{\text{pr}} - t_0$, the nonequilibrium optical conductivity is given by [28, 29]

$$\sigma(\omega, \tau) = \frac{j_{\text{pr}}(\omega)}{i(\omega + i\gamma)A_{\text{pr}}(\omega)}, \quad (7)$$

where $A_{\text{pr}}(\omega)$ and $j_{\text{pr}}(\omega)$ are the Fourier transformations of $A_{\text{pr}}(t)$ and $J_{\text{pr}}(t)$ [$= J_{\text{pr}}(t)/L$], respectively. The damping factor $\gamma (= 0.1)$ is introduced when the Fourier transformations are performed due to the finite simulation time. This is also necessary to distinguish the Drude

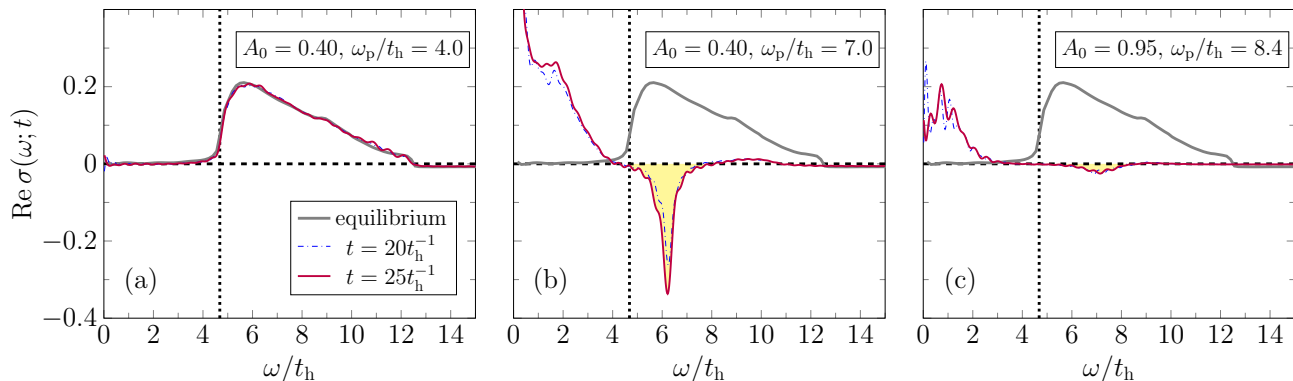


FIG. 2. Nonequilibrium optical conductivity $\sigma(\omega; t)$ for various pump-pulse parameters. The black line is the optical conductivity $\sigma(\omega)$ at equilibrium. The blue (red) line exhibits $\sigma(\omega; t)$ at $t = 20t_h^{-1}$ ($t = 25t_h^{-1}$), respectively. The vertical dotted line denotes the position of the Mott gap, $\omega_p = \Delta_c$.

component of the spectral weight in the limit $\omega \rightarrow 0$. In this paper, we rewrite Eq. (7) as $\sigma(\omega; t)$ with redefining $t = t_0^{\text{Pr}} = t_0 + \tau$ to compare the result of pair correlation functions shown in Fig. 1.

Note that the expectation value of $\hat{J}(t)$ in (quasi-) 1D systems can be simulated directly in the thermodynamic limit by iTEBD, which allows us to observe $\sigma(\omega, \tau)$ for $L \rightarrow \infty$, i.e., in the absence of finite-size and boundary effects. For more details, see Ref. [30].

Figure 2 shows the optical conductivity $\sigma(\omega; t)$ after pulse irradiation ($t = 25t_h^{-1}$) in the η -pairing non-dominant (a) and dominant (b) regimes in addition to the doublon-dominant region (c). In the panel (a) for $\omega_p/t_h = 4.0$ and $A_0 = 0.40$ [marked in Fig. 1 as ‘ \times ’], where the pair correlation $P(r, t)$ doesn’t enhance, $\sigma(\omega; t)$ is almost equivalent to the one in equilibrium as expected. Namely, the spectral weight becomes positive finite above the Mott gap ($\omega_p \gtrsim \Delta_c$ with $\Delta_c/t_h \simeq 4.68$ for $U/t_h = 8$, see the vertical dotted line) and $\sigma(\omega; t)$ are almost equal to the optical conductivity at equilibrium $\sigma(\omega)$. Moreover, $\sigma(\omega; t)$ is rarely time-dependent, consistent with the former results of photoemission spectra at nonequilibrium [21]. The situation changes significantly in the η -pairing dominant regime as in Fig. 2(b) for $A_0 = 0.4$ and $\omega_p/t_h = 7.0$ (marked as ‘+’ in Fig. 1). After pump-pulse irradiation, the spectral weight above the Mott gap is not positive at all but negative. Most remarkably, it exhibits a sharp peak structure, which differs from the former results of the Hubbard model in infinite dimensions [31, 32]. The small enhancement of the pair correlations occurs also around $\omega_p \approx U$ due to the doublon formation [Fig. 1(b)]. The double occupancy $2n_d(t)$ is most enhanced around $A_0 \approx 0.95$ and $\omega_p/t_h \approx 8.4$ marked as ‘ \diamond ’ in Fig. 1. With this pump-pulse parameter set, $\sigma(\omega; t)$ is also not positive for $\omega_p \gtrsim \Delta_c$ as in the η -pairing dominant regime, but the spectral weight is only slightly negative as shown in Fig. 2(c). Thus, the negative conductivity with a sharp peak structure can

be a fingerprint of the photoinduced η -pairing state in pump-probe experiments. Importantly this contradicts previous interpretation of the negative conductivity as coming purely from doublon-hole recombination [31, 32]. In the following, we demonstrate that the photoinduced η pairs can be searched by integrating out the (negative) spectral weight of $\sigma(\omega, t)$ for $\omega \gtrsim \Delta_c$.

Note that in Ref. [31] Li et al. discussed the Drude weight D , which is given by $\text{Re} \sigma(\omega) \sim D\delta(\omega)$, since this relates to the η pair correlations as $D = 4J_{\text{ex}} \langle \hat{\eta}_j \cdot \hat{\eta}_\ell \rangle$ with $J_{\text{ex}} = 2t_h^2/U$. Unfortunately, it costs much more computational effort to simulate $\text{Re} \sigma(\omega)$ in the limit $\omega \rightarrow 0$ since the larger time simulations with keeping the appropriate accuracy are necessary by iTEBD. This task remains a subject for future work.

Now, we simulate the nonequilibrium optical conductivity $\sigma(\omega; t)$ for various pump-pulse parameters A_0 and ω_p and integrate out the spectral weight of $\sigma(\omega; t)$ for $\omega > \Delta_c$ as $f(t) \equiv \int_{\omega > \Delta_c} d\omega \text{Re} \sigma(\omega; t)$. Figure 3 demonstrates the contour plot of $f(t)$ of the model (1) after pulse irradiation, in which the two-peak structure appears. The position of the highest peak coincides with that of the η -pair correlations in Fig. 1(a) (marked as ‘+’), implying the strong relation between the negative conductivity and the formation of η pairs due to the population inversion by pump-pulse irradiation. Examining the negative conductivity sharpens also the second peak around $A_0 = 0.84$ and $\omega_p/t_h = 7.0$, which was unclear in Fig. 1(a). This extra peak can be reconfirmed by exploring the modified structure factor $\tilde{P}_{r>0}(q, t) = \sum_{r>0} e^{iqr} P(r, t)$ in order to get rid of the contribution of local pairs (doublons) from $\tilde{P}(q = \pi, t)$ as demonstrated in Ref. [33]. In Fig. 3(b), we show the contour plot of $P_{r>0}(q = \pi, t) \equiv \sum_{r>0} e^{iqr} P(r, t)$ in the A_0 - ω_p plane. Compared with Fig. 1(a), the two-peak structure is more clearly visible. In addition, the positions of the two peaks agree very well with those obtained from Fig. 3(a), further indicating that the longer-range

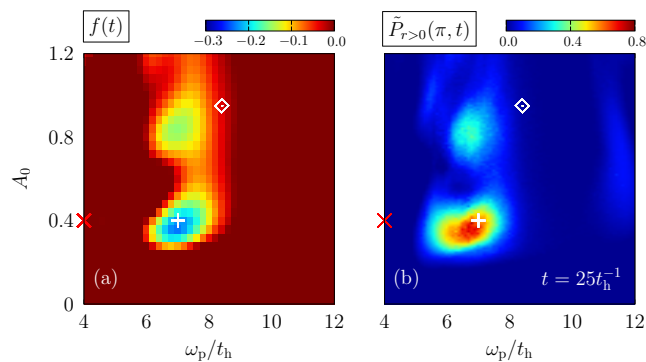


FIG. 3. Contour plot of the integrated negative spectral weight $f(t)$ (a) and the modified structure factor $\tilde{P}_{r>0}(q = \pi, t)$ (b) at $t = 25t_h^{-1}$ in the A_0 - ω_p plane for an infinite Hubbard chain at half filling with $U/t_h = 8$.

correlations play a peculiar role in the η -pairing dominant regime and are directly related to the negative dynamic conductivity.

Figure 4 demonstrates the time dependence of the integrated negative weights with the pump-pulse parameters $A_0 = 0.4$ and $\omega_p/t_h = 7.0$, i.e., the η -pairing dominant point denoted as '+' symbol in Figs. 1 and 3. A clear oscillation can be seen here with the period $T \approx 1/t_h$, which gives us the frequency $\omega' = 2\pi/T \simeq 6.28$, showing a reasonable agreement with the negative peak position $\omega/t_h \approx 6.2$ [see Fig. 2(b)]. This is similar to the oscillations of the optical conductivity due to the Higgs mode [34–39], with respect to the time delay between pump and probe pulse. Since the Higgs is a charge neutral mode it does not couple to linear optical probes and requires an impulsive excitation in nonequilibrium via a nonlinear process. The oscillation is intrinsic to the superconducting state, as the pump pulse is already finished at that point.

Higgs-mediated optical amplification was recently reported for the light-induced superconducting state out of metallic K_3C_{60} and requires a prompt quench [40] which was followed by an observed negative conductivity below 10 meV. In our case the superconducting state emerges from a Mott insulator, which leads to a negative conductivity above the Mott gap.

To sum up, we studied the nonequilibrium optical conductivity of the half-filled Hubbard model in one dimension, by utilizing the unbiased tensor-network algorithm in the infinite matrix-product-state representation. In the photoinduced η -pairing dominant regime the spectral weight becomes significantly negative with a sharp peak structure, reflecting the formation of η pairs. This is a smoking gun to detect the photoinduced η -pairing state of the Hubbard model in spectroscopy experiments since the negativity in the doublon-dominated region is strongly suppressed. Most significantly, by analyzing the time dependence of the negative weight at the η -

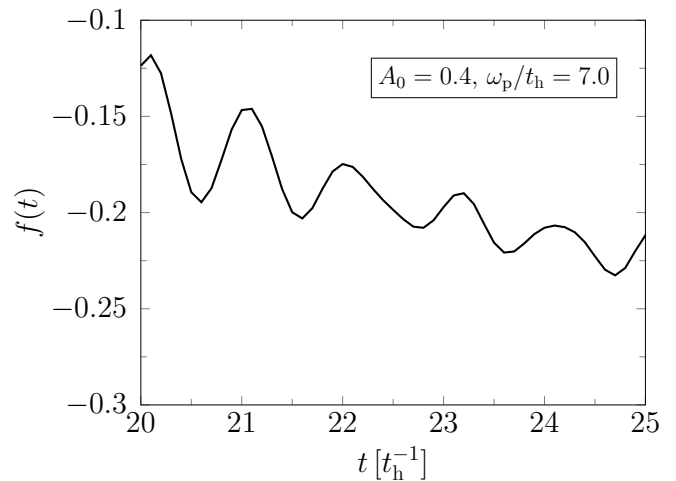


FIG. 4. Time dependence of the integrated negative weights $f(t)$ at the η -pairing dominant point [$A_0 = 0.4$ and $\omega_p/t_h = 7.0$ denoted as '+' symbol in Fig. 3].

pairs most dominant point, a significant oscillation has been observed, reflecting a Higgs-mediated optical amplification due to the non-equilibrium η -pair condensation. Further investigation of this characteristic oscillation is highly desirable.

In the 1D Hubbard model, the spectral weight of $\sigma(\omega; t)$ becomes significantly negative even with the sharp peak structure in contrast to those in the Bethe lattice [31]. Hence, it would be of particular interest to study those in the two-dimensional Hubbard model, e.g., by employing exact diagonalization, to prove the effect of dimensionality.

As demonstrated in Ref. [41] using the exact-diagonalization method, the study of the photoinduced η -pairing state in the Hubbard model can also be applied to the Δ -pairing state in the extended Falicov-Kimball model for spinless fermions, as also confirmed by iTEBD directly in the thermodynamic limit [42]. The negative dynamic conductivity is expected to be observed in the Δ -pairing dominant region of the extended Falicov-Kimball model after pulse irradiation.

Acknowledgments — The authors thank K. Sugimoto for fruitful discussions. This project was made possible by the DLR Quantum Computing Initiative and the Federal Ministry for Economic Affairs and Climate Action; qci.dlr.de/projects/ALQU. The authors gratefully acknowledge the scientific support and HPC resources provided by the German Aerospace Center (DLR). The HPC system CARO is partially funded by "Ministry of Science and Culture of Lower Saxony" and "Federal Ministry for Economic Affairs and Climate Action".

The iTEBD simulations were performed using the ITensor library [43].

-
- [1] C. Giannetti, M. Capone, D. Fausti, M. Fabrizio, F. Parmigiani, and D. Mihailovic, *Adv. Phys.* **65**, 58 (2016).
- [2] S. Ishihara, *J. Phys. Soc. Jpn.* **88**, 072001 (2019).
- [3] A. de la Torre, D. M. Kennes, M. Claassen, S. Gerber, J. W. McIver, and M. A. Sentef, *Rev. Mod. Phys.* **93**, 041002 (2021).
- [4] E. J. Sie, C. M. Nyby, C. D. Pemmaraju, S. J. Park, X. Shen, J. Yang, M. C. Hoffmann, B. K. Ofori-Okai, R. Li, A. H. Reid, S. Weathersby, E. Mannebach, N. Finney, D. Rhodes, D. Chenet, A. Antony, L. Balicas, J. Hone, T. P. Devereaux, T. F. Heinz, X. Wang, and A. M. Lindenberg, *Nature* **565**, 61 (2019).
- [5] J. W. McIver, B. Schulte, F.-U. Stein, T. Matsuyama, G. Jotzu, G. Meier, and A. Cavalleri, *Nature Physics* **16**, 38–41 (2019).
- [6] A. Kogar, A. Zong, P. E. Dolgirev, X. Shen, J. Straquadine, Y.-Q. Bie, X. Wang, T. Rohwer, I.-C. Tung, Y. Yang, R. Li, J. Yang, S. Weathersby, S. Park, M. E. Kozina, E. J. Sie, H. Wen, P. Jarillo-Herrero, I. R. Fisher, X. Wang, and N. Gedik, *Nat. Phys.* **16**, 159 (2019).
- [7] D. N. Basov, R. D. Averitt, and D. Hsieh, *Nat. Mater.* **16**, 1077 (2017).
- [8] R. Mankowsky, A. Subedi, M. Först, S. O. Mariager, M. Chollet, H. T. Lemke, J. S. Robinson, J. M. Glowina, M. P. Minitti, A. Frano, M. Fechner, N. A. Spaldin, T. Loew, B. Keimer, A. Georges, and A. Cavalleri, *Nature* **516**, 71 (2014).
- [9] M. Mitran, A. Cantaluppi, D. Nicoletti, S. Kaiser, A. Perucchi, S. Lupi, P. Di Pietro, D. Pontiroli, M. Riccò, S. R. Clark, D. Jaksch, and A. Cavalleri, *Nature* **530**, 461–464 (2016).
- [10] M. Buzzi, D. Nicoletti, M. Fechner, N. Tancogne-Dejean, M. A. Sentef, A. Georges, T. Biesner, E. Uykur, M. Dreschel, A. Henderson, T. Siegrist, J. A. Schlueter, K. Miyagawa, K. Kanoda, M.-S. Nam, A. Ardavan, J. Coulthard, J. Tindall, F. Schlawin, D. Jaksch, and A. Cavalleri, *Phys. Rev. X* **10**, 031028 (2020).
- [11] M. Budden, T. Gebert, M. Buzzi, G. Jotzu, E. Wang, T. Matsuyama, G. Meier, Y. Laplace, D. Pontiroli, M. Riccò, F. Schlawin, D. Jaksch, and A. Cavalleri, *Nat. Phys.* **17**, 611 (2021).
- [12] M. Eckstein, M. Kollar, and P. Werner, *Phys. Rev. B* **81**, 115131 (2010).
- [13] N. Bittner, T. Tohyama, S. Kaiser, and D. Manske, *J. Phys. Soc. Jpn.* **88**, 044704 (2019).
- [14] D. M. Kennes, E. Y. Wilner, D. R. Reichman, and A. J. Millis, *Phys. Rev. B* **96**, 054506 (2017).
- [15] S. Paeckel, B. Fauseweh, A. Osterkorn, T. Köhler, D. Manske, and S. R. Manmana, *Phys. Rev. B* **101**, 180507 (2020).
- [16] S. Marten, G. Bollmark, T. Köhler, S. R. Manmana, and A. Kantian, *SciPost Phys.* **15**, 236 (2023).
- [17] C. N. Yang, *Phys. Rev. Lett.* **63**, 2144 (1989).
- [18] T. Kaneko, T. Shirakawa, S. Sorella, and S. Yunoki, *Phys. Rev. Lett.* **122**, 077002 (2019).
- [19] J. Tindall, F. Schlawin, M. Buzzi, D. Nicoletti, J. R. Coulthard, H. Gao, A. Cavalleri, M. A. Sentef, and D. Jaksch, *Phys. Rev. Lett.* **125**, 137001 (2020).
- [20] T. Kaneko, S. Yunoki, and A. J. Millis, *Phys. Rev. Research* **2**, 032027 (2020).
- [21] S. Ejima, F. Lange, and H. Fehske, *Phys. Rev. Research* **4**, L012012 (2022).
- [22] S. Ejima, F. Lange, and H. Fehske, *Eur. Phys. J. Spec. Top.* **232**, 3479 (2023).
- [23] R. Islam, R. Ma, P. M. Preiss, M. Eric Tai, A. Lukin, M. Rispoli, and M. Greiner, *Nature* **528**, 77 (2015).
- [24] A. M. Kaufman, M. E. Tai, A. Lukin, M. Rispoli, R. Schittko, P. M. Preiss, and M. Greiner, *Science* **353**, 794 (2016).
- [25] R. Shimano and N. Tsuji, *Annu. Rev. Condens. Matter Phys.* **11**, 103 (2020).
- [26] G. Vidal, *Phys. Rev. Lett.* **98**, 070201 (2007).
- [27] S. Ejima, T. Kaneko, F. Lange, S. Yunoki, and H. Fehske, *JPS Conf. Proc.* **30**, 011184 (2020).
- [28] C. Shao, T. Tohyama, H.-G. Luo, and H. Lu, *Phys. Rev. B* **93**, 195144 (2016).
- [29] J. Rincón and A. E. Feiguin, *Phys. Rev. B* **104**, 085122 (2021).
- [30] K. Sugimoto and S. Ejima, *Phys. Rev. B* **108**, 195128 (2023).
- [31] J. Li, D. Golez, P. Werner, and M. Eckstein, *Phys. Rev. B* **102**, 165136 (2020).
- [32] S. Ray, Y. Murakami, and P. Werner, *Phys. Rev. B* **108**, 174515 (2023).
- [33] S. Ejima, T. Kaneko, F. Lange, S. Yunoki, and H. Fehske, *Phys. Rev. Research* **2**, 032008 (2020).
- [34] P. W. Higgs, *Phys. Rev. Lett.* **13**, 508 (1964).
- [35] C. M. Varma, *J. Low Temp. Phys.* **126**, 901 (2002).
- [36] R. Matsunaga and R. Shimano, *Phys. Rev. Lett.* **109**, 187002 (2012).
- [37] R. Matsunaga, Y. I. Hamada, K. Makise, Y. Uzawa, H. Terai, Z. Wang, and R. Shimano, *Phys. Rev. Lett.* **111**, 057002 (2013).
- [38] L. Schwarz, B. Fauseweh, N. Tsuji, N. Cheng, N. Bittner, H. Krull, M. Berciu, G. S. Uhrig, A. P. Schnyder, S. Kaiser, and D. Manske, *Nat. Commun.* **11**, 287 (2020).
- [39] L. Schwarz, B. Fauseweh, and D. Manske, *Phys. Rev. B* **101**, 224510 (2020).
- [40] M. Buzzi, G. Jotzu, A. Cavalleri, J. I. Cirac, E. A. Demler, B. I. Halperin, M. D. Lukin, T. Shi, Y. Wang, and D. Podolsky, *Phys. Rev. X* **11**, 011055 (2021).
- [41] R. Fujiuchi, T. Kaneko, Y. Ohta, and S. Yunoki, *Phys. Rev. B* **100**, 045121 (2019).
- [42] S. Ejima, F. Lange, and H. Fehske, *Phys. Rev. B* **105**, 245126 (2022).
- [43] M. Fishman, S. R. White, and E. M. Stoudenmire, *SciPost Phys. Codebases* **4** (2022).